Click to view poster presentation.

Constraining the Dynamic Properties of Faults in Compartmentalized Oligocene Mid-Slope Turbidite Channels*

Amelie Dufournet[1], Christophe Nogaret[1], Nick Lagrilliere[1], Thomas Hauge[2], David Lewis[3], Paula Wigley[1], and Rasmus Lang[1]

Search and Discovery Article #51316 (2016)**
Posted October 31, 2016

*Adapted from extended abstract based on poster presentation given at AAPG 2016 Annual Convention and Exhibition, Calgary, Alberta, Canada, June 19-22, 2016

[1]Maersk Oil Houston, TX, United States (nick.lagrilliere@maerskoil.com)
[2]Consultant
[3]Maersk Oil Aberdeen, UK

Abstract

The reservoir development plan targets several pressure compartments, which are cut by multiple small yet seismically resolved faults. These faults partially disconnect the channels between the planned injectors and producers and their dynamic behaviour is a key uncertainty for the development in the absence of production data. The purpose of this study was to review the data available to constrain the fault sealing and baffling capacity in the field. A review of the geological settings allowed a better understanding of the timing and mechanisms of deformation in the field. Faults formed at different times (Oligocene and Miocene extension, Late Miocene to present day compression) and are not expected to have the same flow characteristics. When deformation occurs at great depth of burial, stress and temperature conditions allow crushing and dissolving sand particles during displacement causing significant permeability reduction in the clay-free areas of the fault zone (where flow preferentially occurs). Fault seal analysis was performed integrating reservoir fluid pressures measurements, seismic DHI and structural/stratigraphic observations. Faults appear to leak over geological time in areas where they juxtapose thick sand units at the base of the channels. This explains the presence of a laterally extensive aquifer penetrated by 3 wells in different compartments. Elsewhere, faults throw and shale gauge lead to pressure disconnection of oil sands. Deformation features seen in cores were classified and measured, leading to the definition of three permeability/capillary entry pressure functions related to the fault clay percent. The different permeability/capillary entry pressure functions are utilised for faults of different ages. Early faults (formed at less than 1 km of burial depth) are open in clay free areas (as suggested by flatspot continuity across them). Large Miocene faults are baffling in clay-free areas and can hold minor pressure differences (10-40 psi). Faults related to the late contraction are strongly baffling in clay free areas and can hold major pressure difference between compartments (>100 psi). The fault permeability in clay free areas is thus constrained by the age of the fault and the fault seal analysis. Uncertainty remains on the estimation of fault shale gauge ratio which determines which areas of the faults are clay free and open, baffling (20 to 40% shale gauge ratio) or sealing (more than 40% shale gauge ratio).

Introduction

The study area is located on the present-day Angolan shelf slope in the Lower Congo Basin, which forms part of a passive margin characterized by overburden rafting and salt diapirism. It is part of a post-salt Cretaceous to Oligocene raft (Mega-Raft N) separated from the Mega-rafts E and S by Miocene Depocenters (respectively Depocenter 1 and 4 in Figure 1). Due to the topography of the basement beneath the decollement salt layer, the area is structurally deeper than and partially disconnected from the rest of Mega-Raft N to the East. The Western part transitions to the compressional domain of the margin characterized by salt diapirism and salt mini-basins. The area has several stacked Oligocene mid-slope turbidite channels in different pressure compartments, which are cut by small yet seismically resolved faults with displacement of up to 40 meters (Figure 2). These faults partially disconnect potential reservoir flow units in the channels and in the area in the absence of production data, their impact during production is a key uncertainty to any development (Figure 3). The purpose of this study was to review the data available to constrain the fault sealing and baffling capacity in the area.

Timing and Mechanisms of Deformation in the Field

Analysis of isochore maps (Figure 4) and seismic sections (Figure 5) shows that faults formed at different times, corresponding to different burial depths.

Cretaceous to Early Miocene: Phase 1 Rafting

As the South Atlantic Ocean started to spread, the carbonate overburden began to stretch in the Middle to Late Cretaceous forming many small rafts sliding over a relatively thick salt layer and rotating along minor listric faults. Accommodation space in the study area was created by displacement of the deeper salt, preferentially on the eastern side of the raft but with some variations through time, as the salt was expelled to the north and/or the south. Several remnant salt rollers (with typical triangular shapes in cross-sections) associated with this early rafting episode are still observable in the area (Figure 5). Faults coloured in red in Figure 2 are antithetic to this eastern listric fault. Faults coloured in orange are probably related to a similar system in the West, but were reactivated during later deformation.

During the Cretaceous, the central salt diapir was actively rising as the sediments were deposited, causing the observable curvature of the seismic reflectors at the salt-sediment interface (see seismic section in Figure 5). During the Oligocene, the sedimentation rate increased whereas the rate of the salt rise decreased. The salt structure still constituted a local high: the E-W oriented turbiditic channel systems flowed around it on either the northern or southern flanks, resulting in thinner deposits over the salt diapir itself (Figure 4) and the arched geometry of the seismic reflectors (Figure 5). During the Late Oligocene, the central salt diapir started to collapse. Several small reactive crestal faults radiated from the salt structure, and allowed for local thickening of the Upper Oligocene sediments (Figure 4). The topography imposed by the central diapir was leveled during the Early Miocene, as proven by the flat geometry of the Mid-Miocene seismic reflector over the salt dome (Figure 5).

Formation of the Miocene depocenters: Phase 2 Rafting

During the Miocene, larger mega-rafts formed by amalgamation of several older mini-rafts consolidated by the overlying Oligocene units (Figure 1). Miocene sediments accumulated in trough-like depocentres lying directly on the salt between Mega-raft N and the surrounding mega-rafts: a major NNW-SSE elongated trough was located far to the east of the study area along with the smaller perpendicular Miocene trough immediately to the east (Figure 1 and Figure 5). Extension thus occurred both parallel and perpendicular to the margin slope due to gravity spreading under the weight of the sediments over a salt layer and in reaction to particular basement topography and structure. The north-south extension was dominant in the study area. Major E-W oriented faults and associated smaller antithetic and transfer faults formed several horst/graben structures allowing massive Miocene sediment deposition to the east (Figure 4). The faults are deflected by the central salt dome, which caused a different local stress regime.

Late Miocene to present day: Compression and salt diapirism

During the late Miocene, the raft moved over the basement structural high (currently located east of the field in Figure 1) as it continued to slide over the salt layer. The transition to a basement structural low caused the current westward dip observable on the Miocene unconformity (Figure 5). The Pliocene sediments onlap onto this unconformity (Figure 5) and thicken to the west (Figure 4). Salt diapirs formed NE, NW and SW of the area and formed turtle structures in the Pliocene sediments as the salt evacuated and rose. The western side of the raft reached the compressional domain of the passive margin. Faults on this side were reactivated as reverse faults. The rest of the area behaved as a coherent unit with no apparent internal deformation during this period, as suggested by the termination of the faults at the Miocene unconformity (Figure 5).

In conclusion, the faults mapped in the Oligocene section can be classified in three age categories (Figure 6):

- The early faults, active during the Oligocene and Lower Miocene, when the sediments were at near surface or shallow burial depths (< 1 km): probably the ones related to the central salt dome and the small short-lived antithetics of the major E-W faults,

- A few faults that continued to be active throughout the Miocene (dark blue faults on Figure 2). This corresponds to a burial depth of up to 1.5 km for the Upper Oligocene sediments, and up to 2 km for the Lower Oligocene sediments. Those major E-W oriented faults are interpreted to constitute the vertical conduit that allowed the migration of oil (by stair stepping from the Cretaceous source rock to the Oligocene) and to be the architects of the fluid pressure regimes in the area.

A few faults that were reactivated during the late compression at a greater depth of burial (more than 2 km) on the western side of the area (orange on Figure 2).

Data Available to Constrain the Faults Sealing and Baffling Capacity in the Field

Fault damage zones are complex, heterogeneous and anisotropic volumes of varying structure and lithological content, controlled by the shale gauge ratio and grain size of the host rock as well as syn- and post-deformation stress and temperature history (Figure 6, from Reference 3). When deformation occurs at a depth of burial >1km, stress and temperature conditions allow for crushing and dissolution of sand particles

during displacement, causing significant permeability reduction in the clay-free areas of the fault zone (where flow preferentially occurs). Under similar burial conditions, faulted clay-rich sands (15-40% clay content) form a PPFG (Phyllosilicate framework) with clay particles mixing with the framework grains. The clay minerals enhance quartz dissolution in the fault zone even after the faulting event, resulting in porosity and permeability reduction within the fault zone. The finer-grained materials also give high 'capillary entry' or 'threshold' pressures and can lead to the separation of Oil Water Contacts (OWC) across hydrocarbons accumulations. Faulted shale beds result in the formation of clay smear entrained within the fault zone that may act as a local seal. All these mechanisms can have a profound effect on the variability of sealing/baffling behaviour of faults within a reservoir during field production time.

A few deformation features were observed in cores from the study area (Figure 7): the most prominent deformation fabric observed was sheared sections of sand and shale, likely caused by gravity slumping or sand injection in unconsolidated sediments during or shortly after deposition. Some features were interpreted to be associated with later deformation in consolidated rocks (discrete breaks and deformation bands) but none could be related to a seismically interpreted fault. Permeability, capillary entry pressure and clay percent were measured in several core samples, leading to the definition of three permeability/capillary entry pressure functions related to the fault clay percent and burial depth (Figure 8 and Figure 9).

As illustrated in Figure 8, "Early" faults (formed at less than 1 km of burial depth) are interpreted to be open to fluid flow in clay free areas (self-juxtaposition of thick sand units). "Later deformation-Shallow reservoir" faults (active up to 2 km of burial depth) are baffling and may hold minor pressure differences (10-40 psi) in clay-free areas. "Later deformation-Deep reservoir" faults (active at more than 2km of burial depth) are strongly baffling and can hold major pressure difference between compartments (>100 psi) in clay free areas. The results of flow tests from wells in the area cannot be used to calibrate the faults transmissibility. However, the variability of the faults sealing/baffling behaviour based on the core measurements can be validated by a fault seal analysis, integrating reservoir fluid pressures measurements, seismic Direct Hydrocarbon Indicator (DHI) and structural/stratigraphic observations.

All faults appear to leak over geological time in areas where they juxtapose thick sand units at the base of the channels (Figure 10). This explains the presence of a laterally extensive aquifer penetrated by wells in three different compartments. Elsewhere, faults throw and shale gauge (PFFR and clay Smear) lead to pressure disconnection of oil compartments: oil pressure differences observed in the different wells range from 10 to 110psi. According to the geological history described in section A (above), faults separating pressure compartments with minor pressure difference (10-40 psi) were active during the Miocene while faults separating the western compartment (C4) from the rest of the field were reactivated during the late compression and can hold larger pressure difference (110psi). A flatspot interpreted on the far seismic data (potential seismic expression of an OWC) was observed crossing 2 faults classified as "Early", suggesting the minimum capillary entry pressure of the faults is less than 3 psi (~5 meters, difference undetectable on seismic).

Fault Sealing and Baffling Capacity Uncertainty

The interpreted fault sealing and baffling behaviours were implemented with the following workflow in the reservoir models in the area:

- Estimation of the fault clay content from the host rock V_{Shale} property and the fault displacement: a number of algorithms exist to represent the mixing of clay particles and smearing of shale layers along the fault plane (Effective Shale Gauge Ratio–ESGR and the Smear factor or simple extraction of the maximum V_{Shale} value from juxtaposed cells). The ESGR algorithm calculates the clay percent at any point along the fault surface as a weighted average of the proportion of shale within the stratigraphy that has slipped past that point, inversely weighted by the distance. The smear factor algorithm produces a binary arrangement of totally sealed and totally open to flow bands across the fault plane, depending on the proximity of cells with $V_{Shale} > 40\%$ along the fault plane.
- Estimation of the fault permeability from the fault clay content using the core-calibrated functions described in section B.
- Calculation of the fault transmissibility, function of the fault permeability, fault thickness and host permeability.

A sensitivity analysis was performed and the resulting tornado plot is presented in Figure 11. The results are relevant for the model resolution and workflow (grid cells are 50mx50mx2m, the geological model was carried to simulation without upscaling and shale cells are inactivated), but may not be representative elsewhere. The most sensitive variable was found to be the proportion of the fault plane sealed by clay mixing and smearing (clay percent>40%) which impacts the ultimate recovery in the models as more or less oil can be trapped along the fault plane: different estimation techniques lead to a variation of 25% in recovery. Another sensitive parameter was the order of magnitude of the permeability reduction in areas of the faults with clay percent less than 40%. The "Later deformation-deep reservoirs" clay percent to permeability function leads to significant flow retardation and the creation of additional traps along the fault plane that reduce the ultimate recovery by about 10% compared to the 2 other functions which lead to similar recovery profiles. Non-sensitive parameters within the considered uncertainty range were varying the fault throw, the fault thickness to displacement ratio and the minimum capillary entry pressure (negligible compared to pressure differences in the reservoir during production).

Conclusions

According to the geological history summarized in sections A and B, the "Later deformation-Deep reservoir" clay percent to permeability functions should not be used to characterize the behavior of the small intra-compartment faults in the area. As shown by the sensitivity analysis in section C, the ultimate recovery is not significantly sensitive to the permeability variations imposed by the two remaining clay percent to permeability functions. We conclude that, for a given static model, the uncertainty on the fault transmissibility is mainly dependent on the fault clay percent estimation technique. We propose to reduce the range of uncertainty (from all faults closed to all faults open) to a narrower range where only the fault clay percent estimation technique varies.

Acknowledgement

The authors gratefully acknowledge the management of Maersk Oil, Odebrecht and Sonangol for permission to publish this work, and would like to thank our colleagues, particularly Kevin Schofield and Raja Mukherjee for reviewing the material presented herein, and RDR now a Schlumberger affiliated company for the core measurements and fitted functions.

Reference Cited

Jolley, S.J., H. Dijk, J.H. Lamens, Q.J. Fisher, T. Manzocchi, H. Eikmans, and Y. Huang, 2007, Faulting and fault sealing in production simulation models: Brent Province, northern North Sea: Petroleum Geoscience, v. 13, p. 321–340.

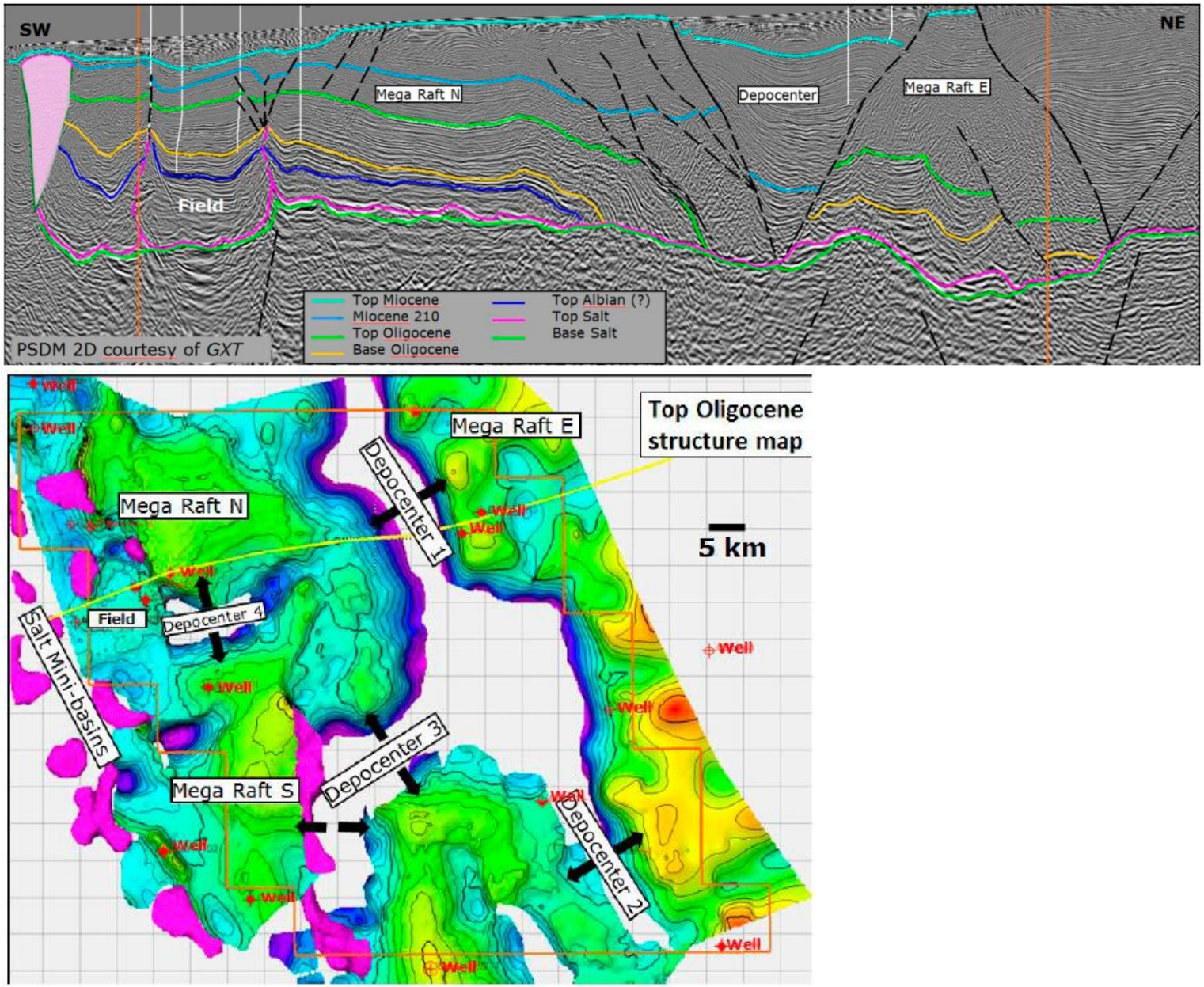

Figure 1. Seismic intersection showing the regional setting and regional structure map of the Top Oligocene (yellow line positions the seismic section interpreted above, pink objects represent salt structures).

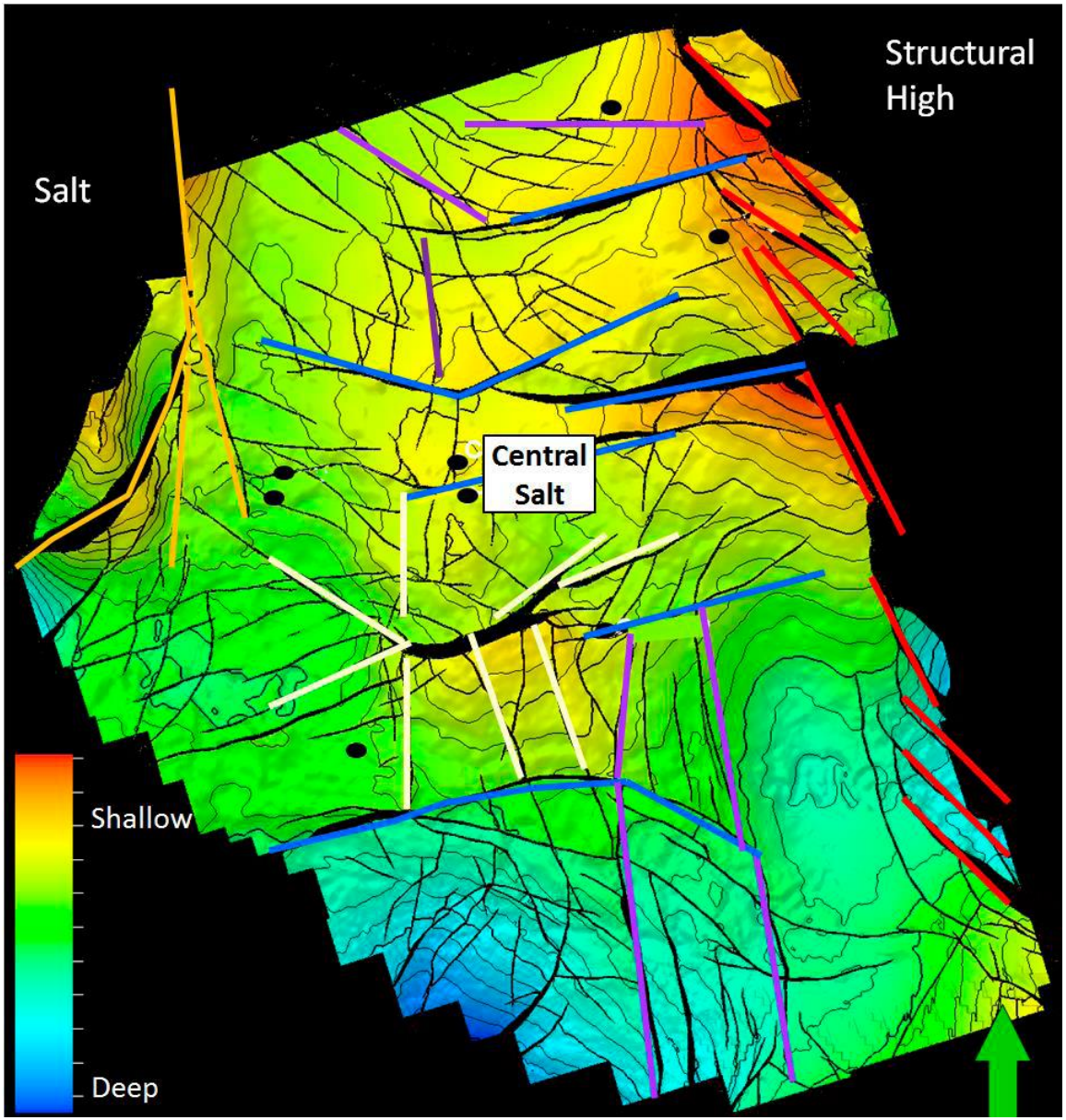

Figure 2. Structural map showing the different fault families observed in and around the study area. In yellow, faults radial to the central dome. In red, faults parallel or oblique to the eastern ridge. In Blue, major Miocene faults and in purple smaller antithetic or transfer faults. In orange, reverse faults circumferential to western Salt dome.

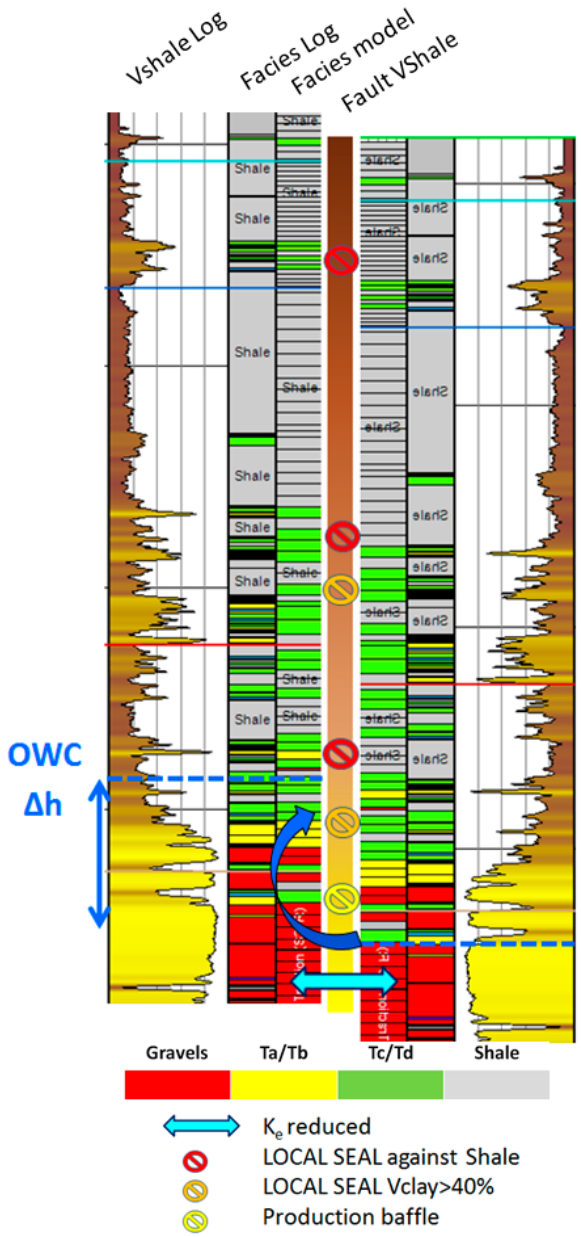

Figure 3. Impact of a 20 meters throw in a typical mid-slope turbidite channel sequence in the area: shale gouge in the fault zone can cause local seals, flow retardation and separation of Oil Water Contacts. Flow and pressure equilibrium are likely to occur at the base of this fining-upward sequence.

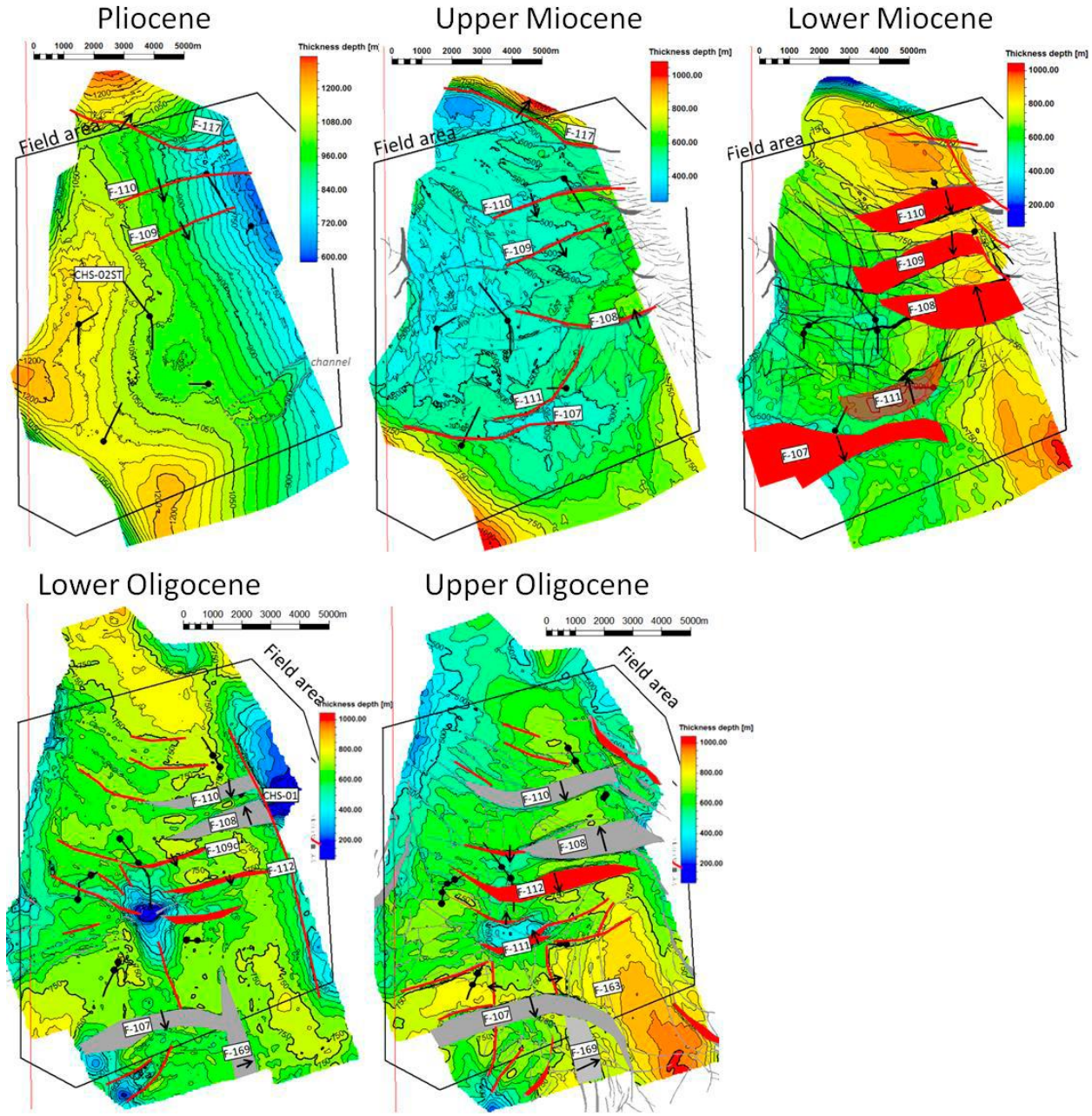

Figure 4. Isochore maps. Faults active during the period are shown in red, inactive in grey. Wells are shown in black with entry and exit point of the stratigraphic interval.

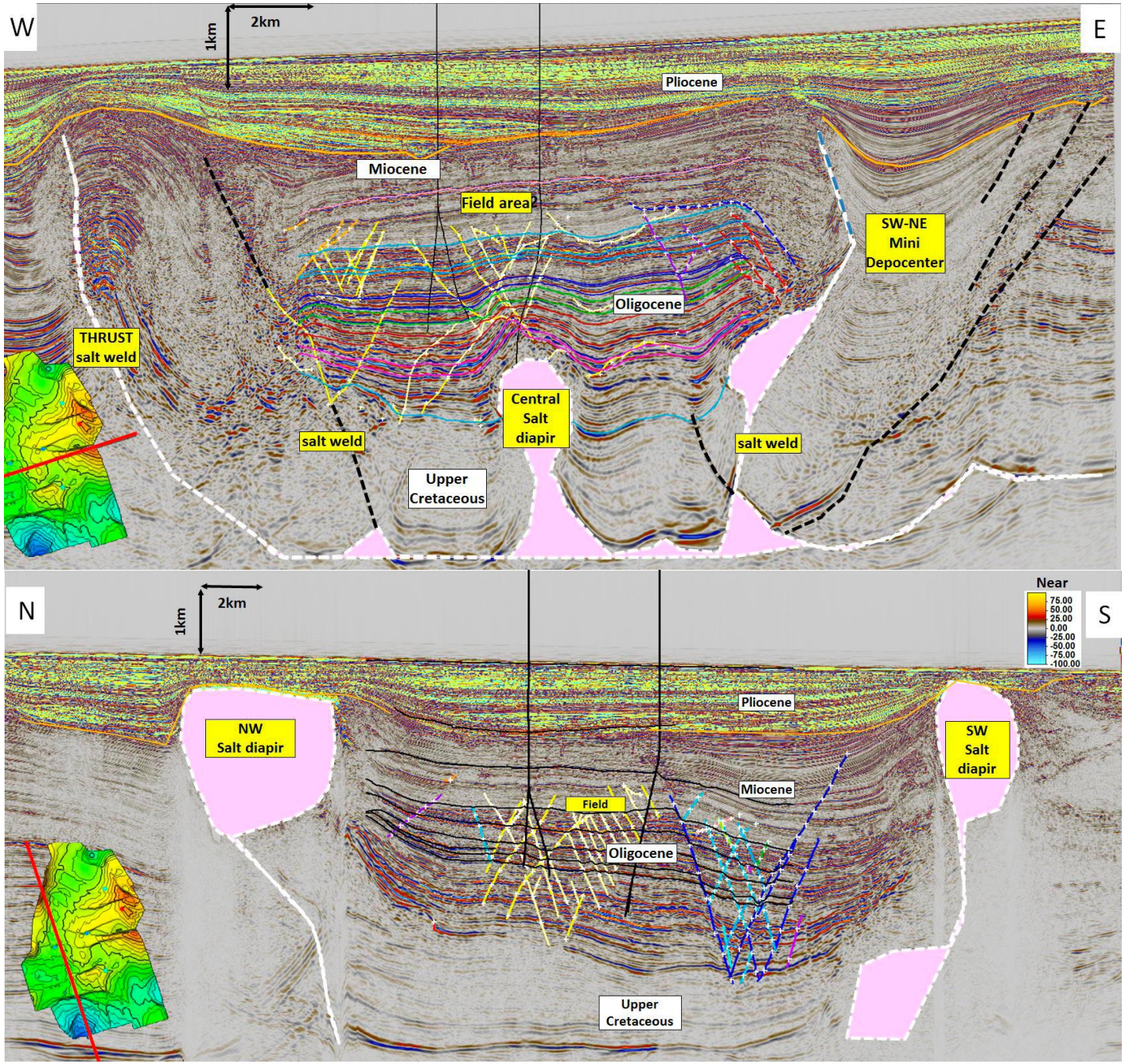

Figure 5. Interpreted E-W and N-S seismic section in the area.

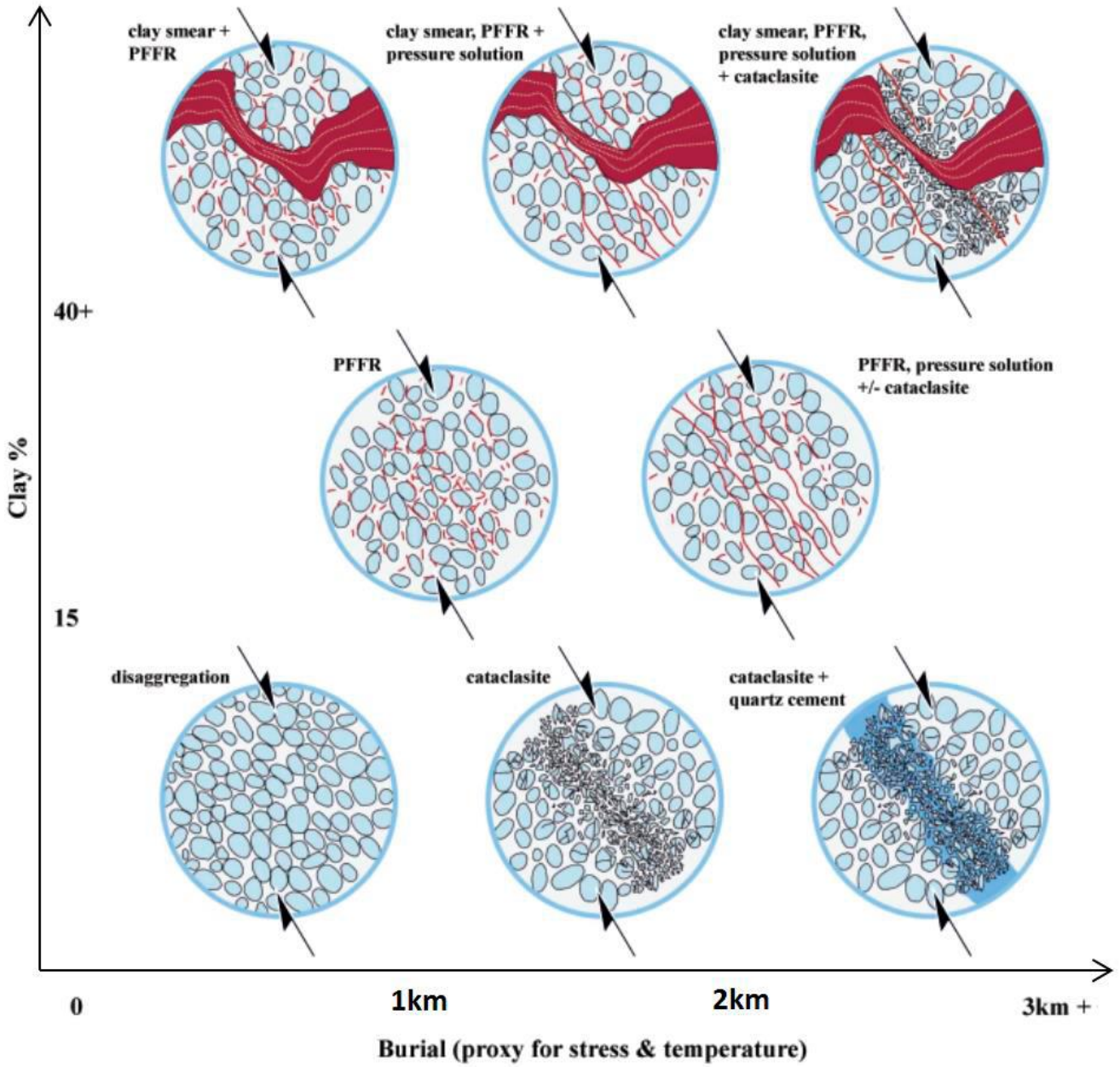

Figure 6. Schematic cartoons of micro-structural processes within fault rocks leading to permanent collapse of the host rock porosity-permeability structure, as a function of host rock shale gauge ratio and burial depth (PPFG: phyllosilicate framework) (Jolley et al., 2007, reference 3).

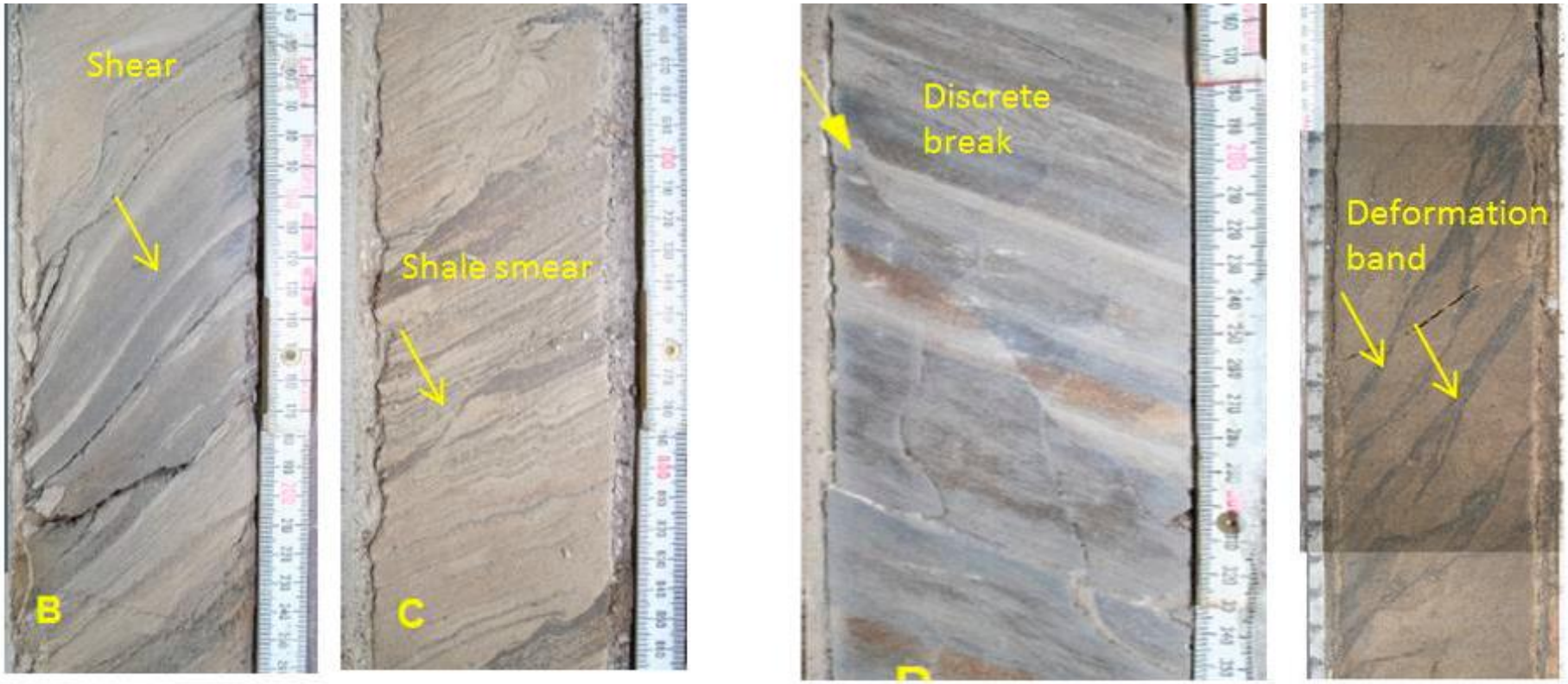

Figure 7. Some deformation features observed in the cores.

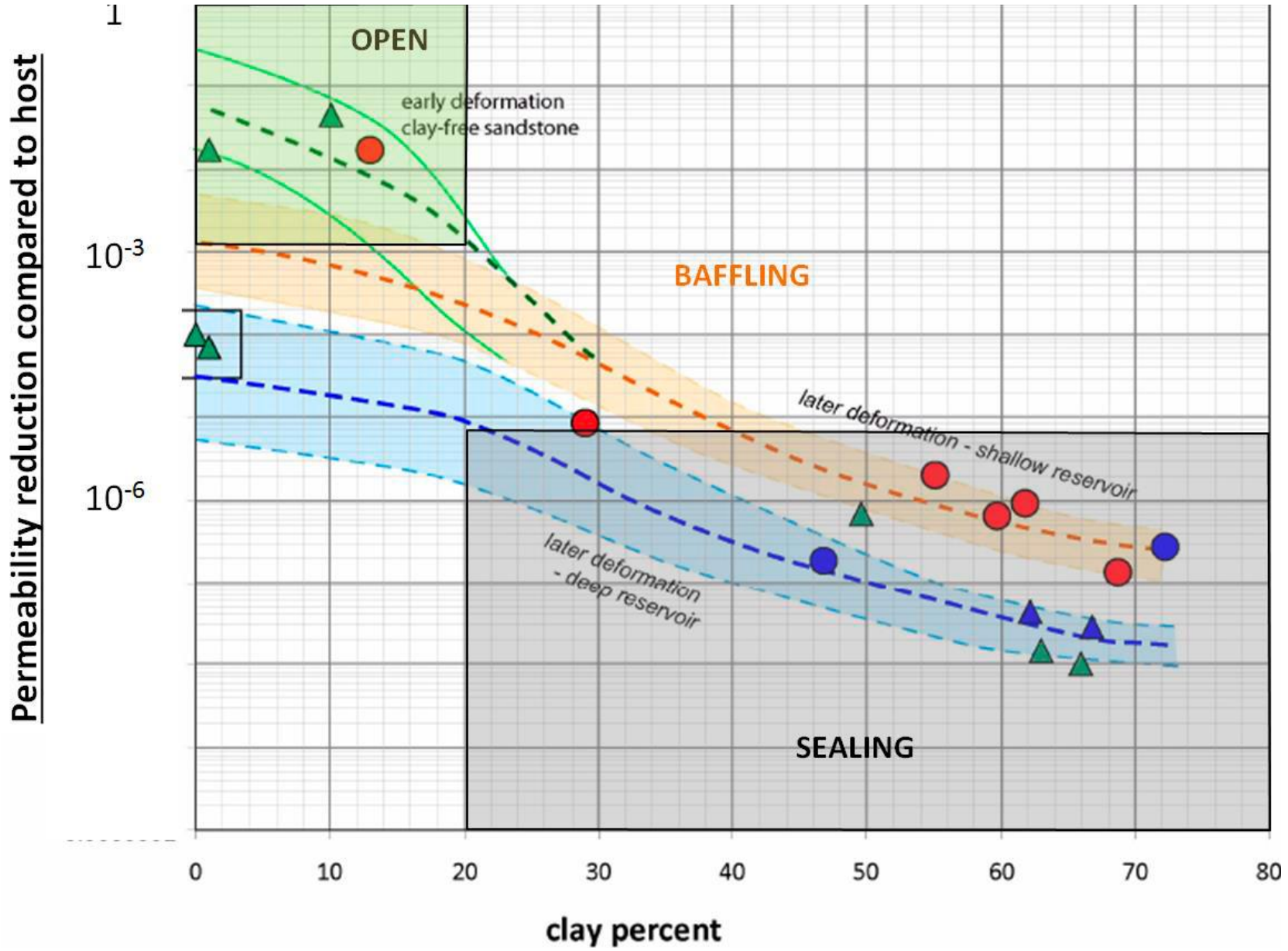

Figure 8. Core measurements of permeability reduction of the deformation samples compared to the host rock plotted against clay percent. Green triangles correspond to samples from deepest interval; red circles to shallowest interval; blue points/circles are samples were permeability is derived from measured Capillary Entry Pressure (core measurements and fitted functions as described in a proprietary study performed by RDR, now a Schlumberger affiliated company).

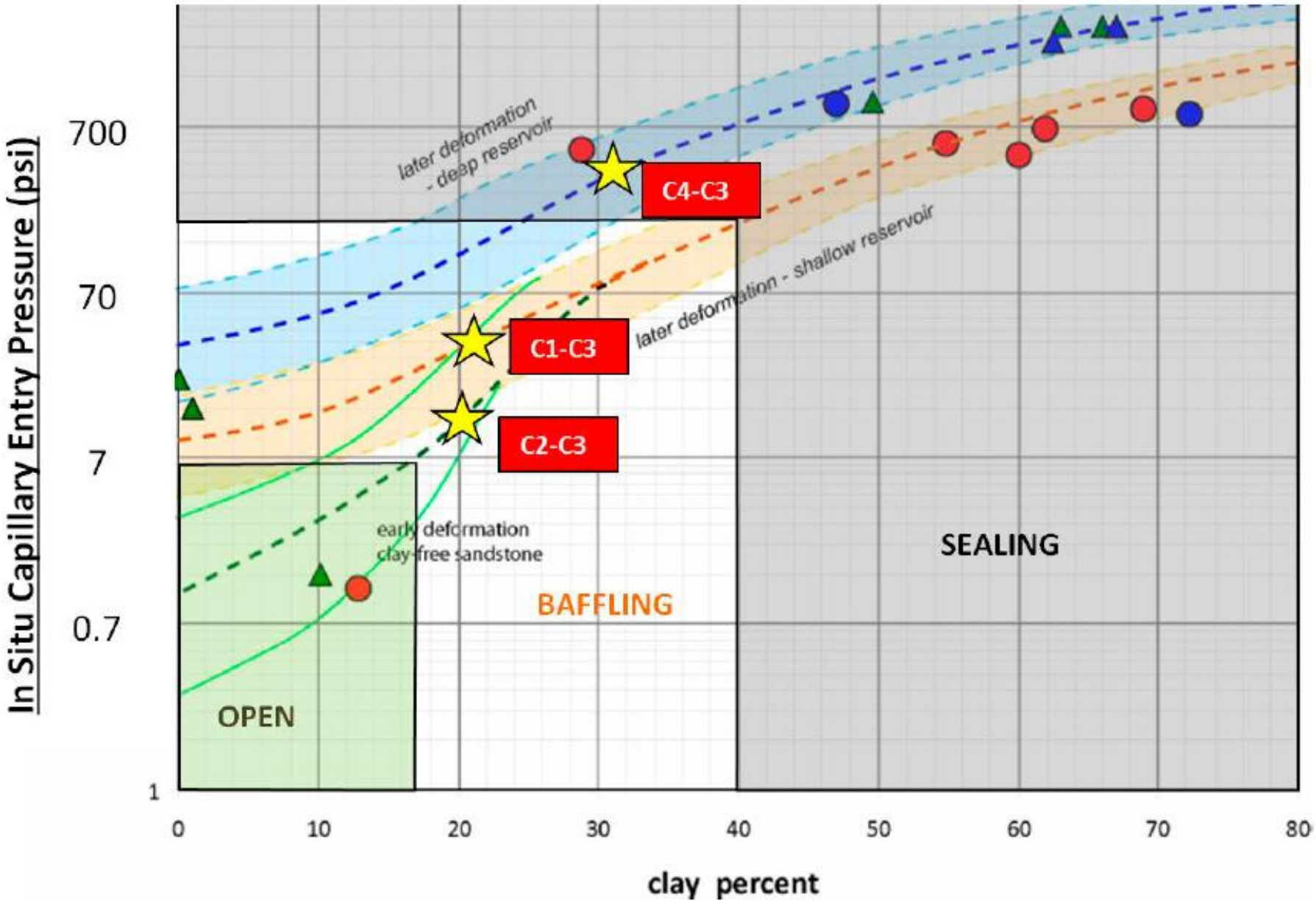

Figure 9. Core measured capillary entry pressure plotted against clay percent of the deformation samples. The yellow stars indicate the pressure difference observed between the pressure compartments (compartment names in red boxes) penetrated by the wells in the area (core measurements and fitted functions by Schlumberger-RDR).

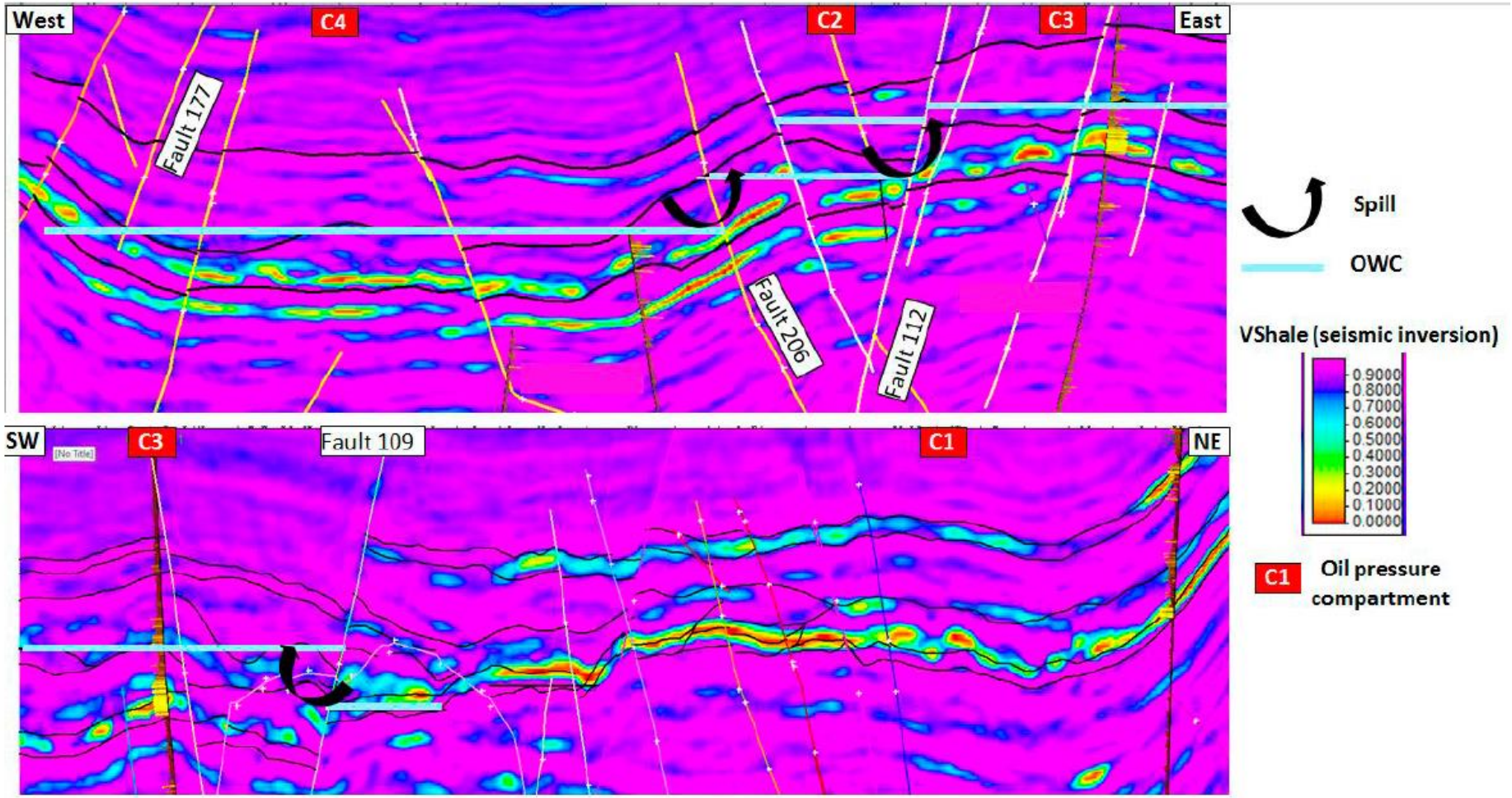

Figure 10. V_{Shale} Inversion Seismic lines showing OWC and spill points between different pressure compartments.

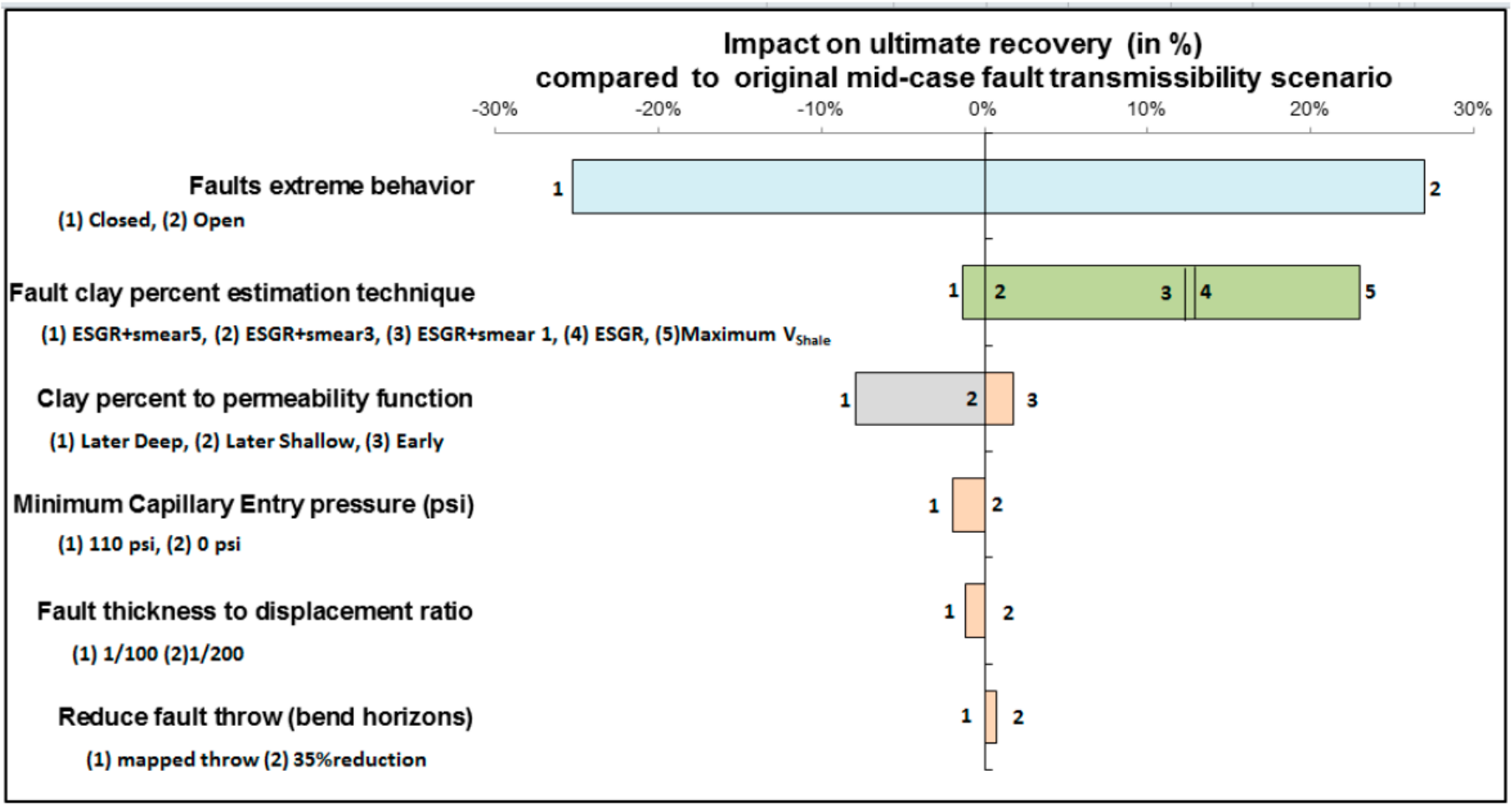

Figure 11. Tornado chart resulting from the sensitivity analysis on the faults transmissibility estimation. Uncertainty can be constrained by a better understanding of the geological history and core data (grey areas excluded from uncertainty range) and of the workflow sensitivity (non-sensitive variable in orange are abandoned).